Supplement of Atmos. Chem. Phys., 23, 15181–15196, 2023
https://doi.org/10.5194/acp-23-15181-2023-supplement

Atmospheric Chemistry and Physics
Open Access

Supplement of

The sensitivity of Southern Ocean atmospheric dimethyl sulfide (DMS) to modeled oceanic DMS concentrations and emissions

Yusuf A. Bhatti et al.

Correspondence to: Yusuf A. Bhatti (yusuf.bhatti@pg.canterbury.ac.nz)

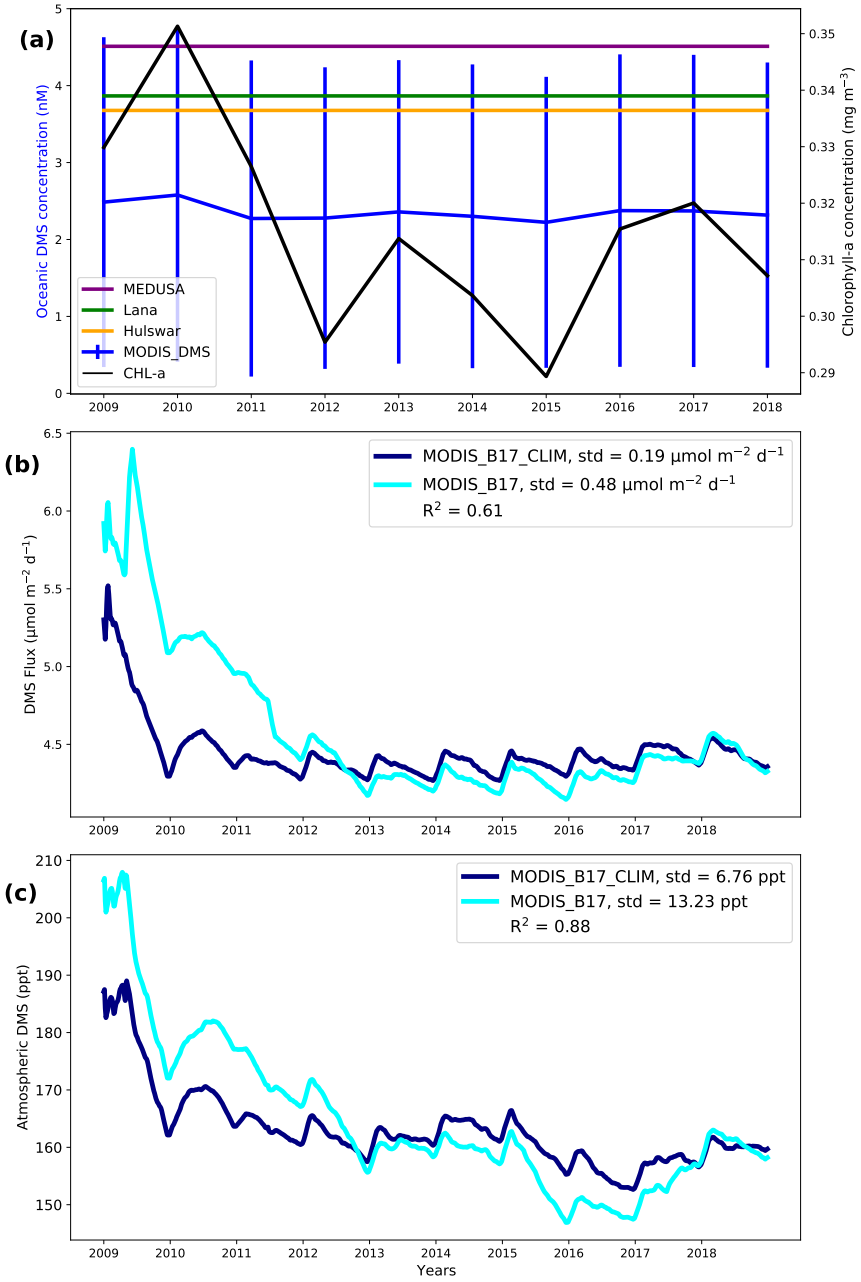

Figure S1. Timeseries of each oceanic DMS dataset input into the simulations during DJF in the Southern Ocean. (a) chl-a is shown with a black line. The MODIS-DMS error bars represent the standard deviation across the Southern Ocean. (b) comparison of the DMS emissions between MODIS$_{B17}$ with the MODIS$_{B17}$CLIM. (c) as (b) but showing the surface atmospheric DMS concentrations. The legend highlights the standard deviation in annual flux, along with the R^2 value between the two simulations. (bottom) as for the (middle) but showing atmospheric DMS concentrations.

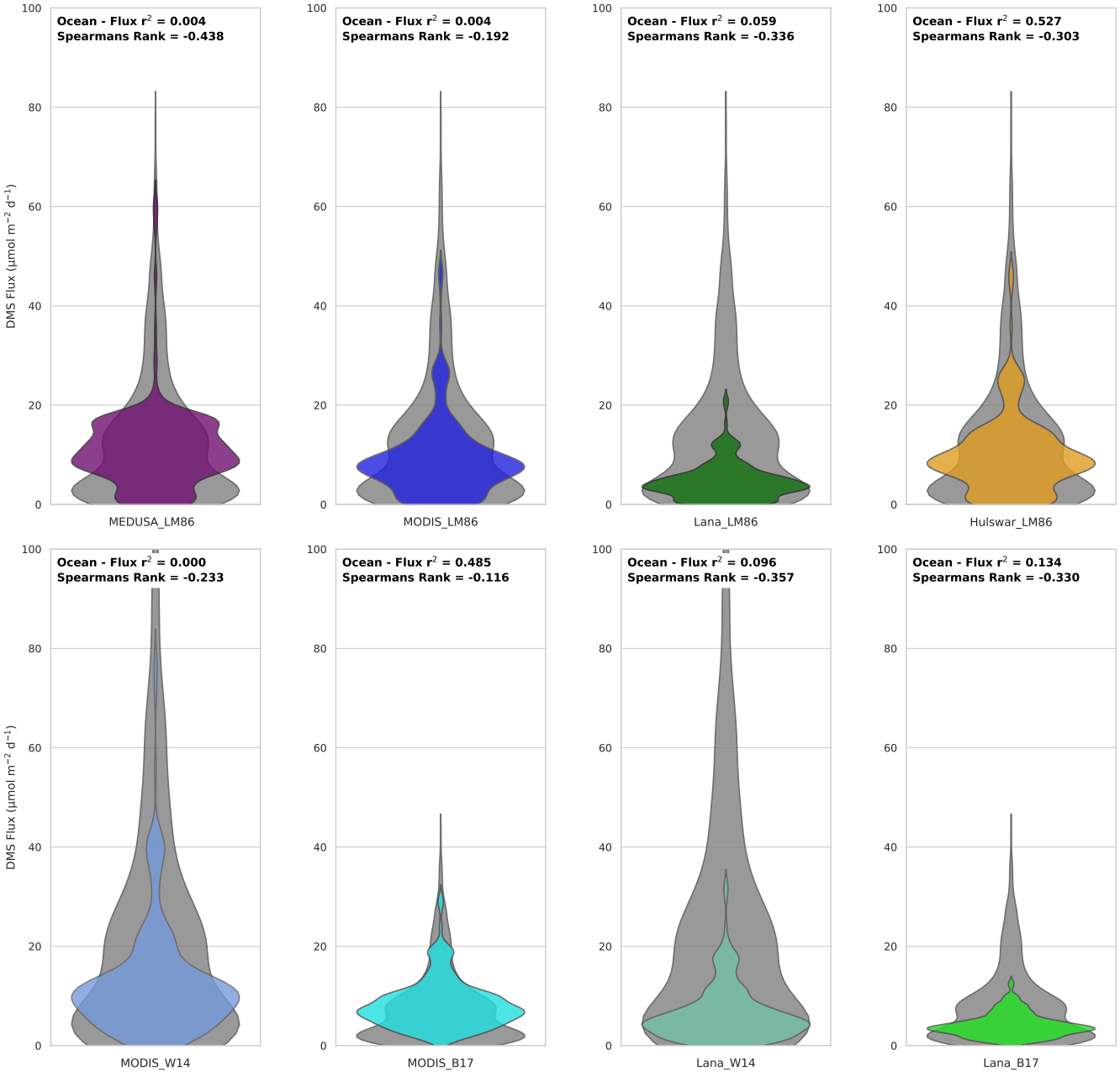

Figure S2. DMS emissions for each simulation following the SOAP voyage across each hour, through time and space as a violin plot. The r^2 value compares the monthly DMS flux against the respective oceanic DMS. Spearman's rank compares the rankings of hourly flux simulation with the rankings of hourly TAN1802 data. Each simulation overlays the corresponding SOAP voyage flux, whereby both emissions are calculated with the same sea-to-air flux, winds, and Schmidt number.

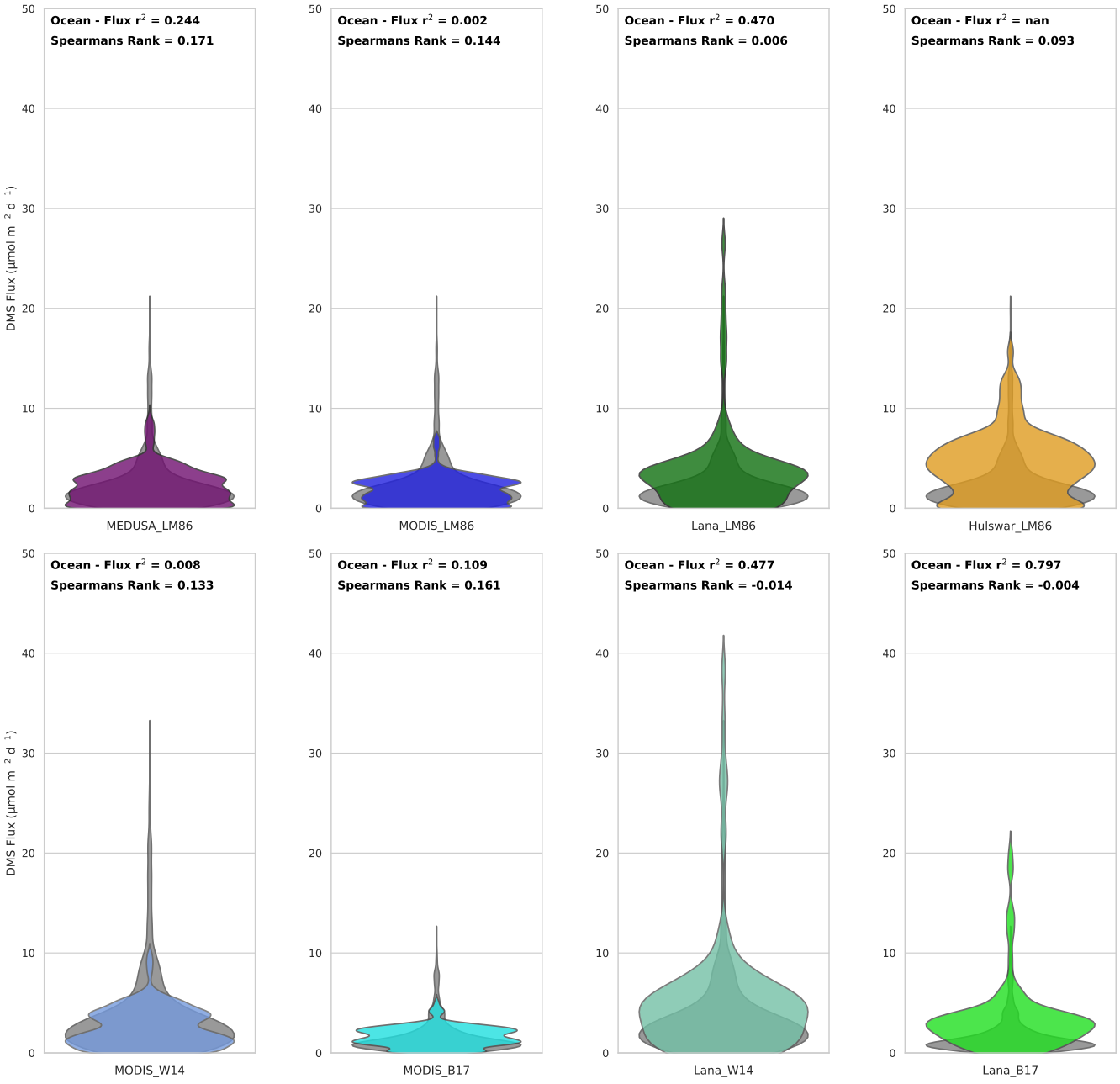

Figure S3. Same as Figure S2, but for TAN1802

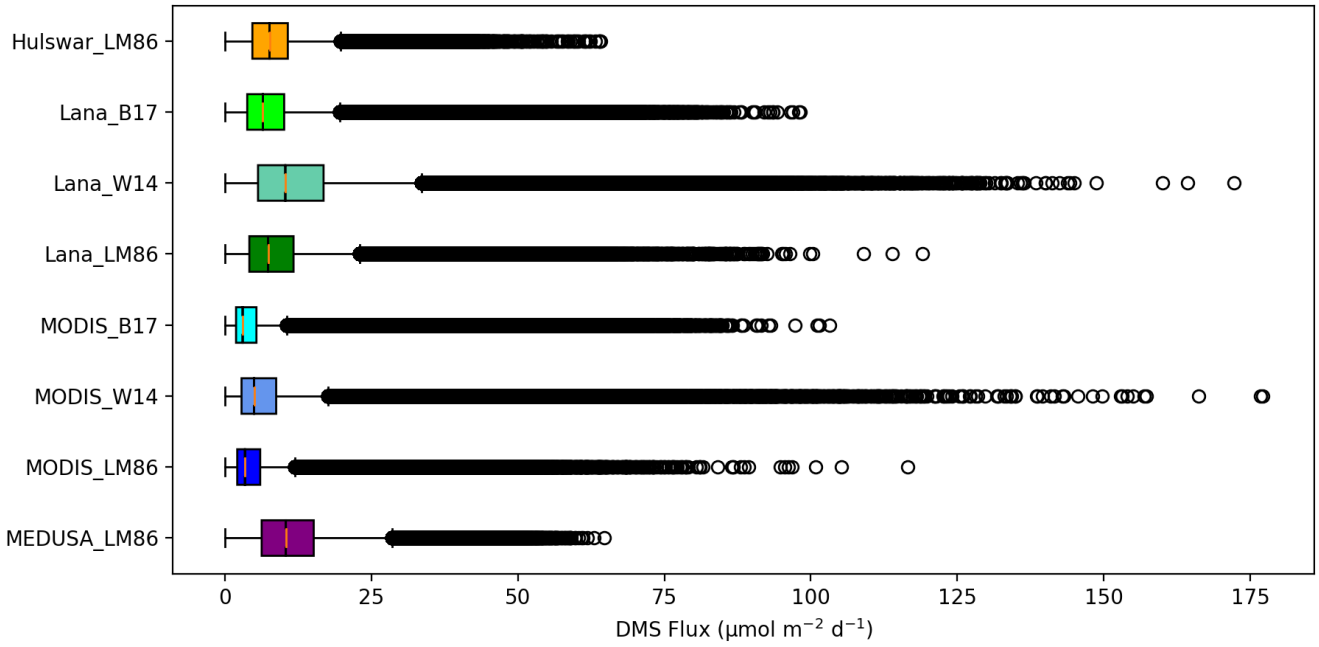

Figure S4. DMS emissions for all simulations over the 10 years using daily data in the summertime (DJF) over the Southern Ocean as a box plot.

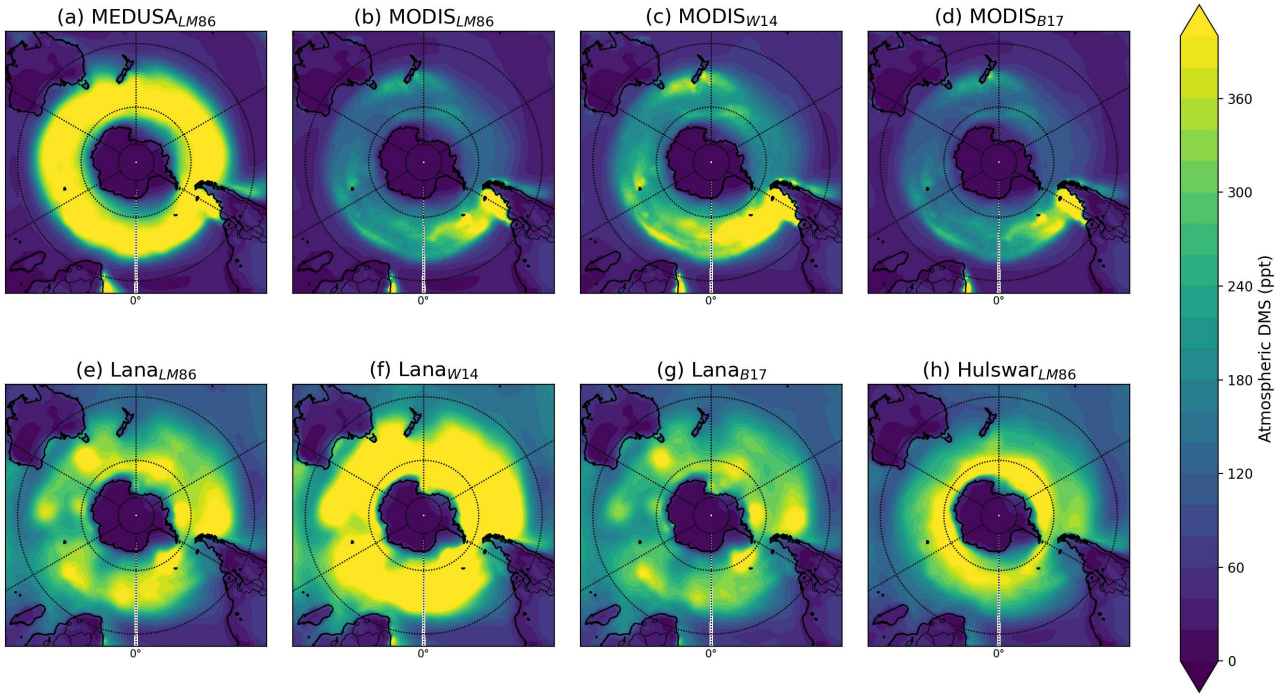

Figure S5. Summertime (DJF) atmospheric DMS concentrations over the Southern Ocean. The spatial distribution shows the simulations with different oceanic DMS concentrations and different DMS flux parameterizations.

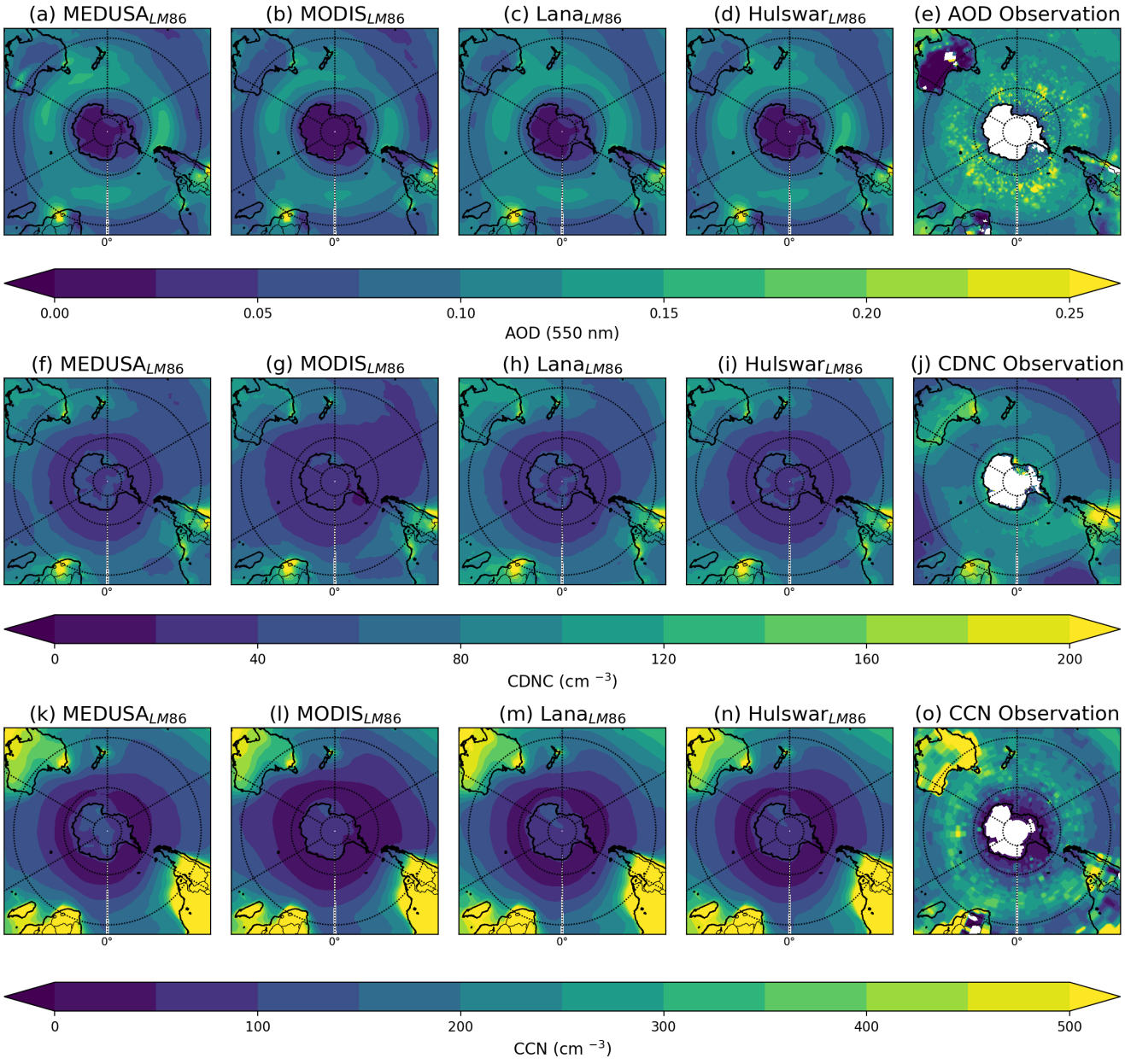

Figure S6. Spatial distribution of each oceanic DMS data set using the Liss and Merlivat (1986) transfer velocity parameterization for (a – d) AOD, (f – i) CDNC, and (k – n) CCN. The observations are from (e) MODIS AOD satellite retrieval, (j) Grosvenor et al. (2018), and (o) the from Choudhury and Tesche (2023).

References

Choudhury, G. and Tesche, M.: A first global height-resolved cloud condensation nuclei data set derived from spaceborne lidar measurements, Earth System Science Data, 15, 3747–3760, https://doi.org/10.5194/essd-15-3747-2023, publisher: Copernicus GmbH, 2023.

Grosvenor, D. P., Sourdeval, O., Zuidema, P., Ackerman, A., Alexandrov, M. D., Bennartz, R., Boers, R., Cairns, B., Chiu, J. C., Christensen, M., Deneke, H., Diamond, M., Feingold, G., Fridlind, A., Hünerbein, A., Knist, C., Kollias, P., Marshak, A., McCoy, D., Merk, D., Painemal, D., Rausch, J., Rosenfeld, D., Russchenberg, H., Seifert, P., Sinclair, K., Stier, P., van Diedenhoven, B., Wendisch, M., Werner, F., Wood, R., Zhang, Z., and Quaas, J.: Remote Sensing of Droplet Number Concentration in Warm Clouds: A Review of the Current State of Knowledge and Perspectives, Reviews of Geophysics, 56, 409–453, https://doi.org/10.1029/2017RG000593, _eprint: https://onlinelibrary.wiley.com/doi/pdf/10.1029/2017RG000593, 2018.

Liss, P. S. and Merlivat, L.: Air-sea gas exchange rates: Introduction and synthesis, in: The role of air-sea exchange in geochemical cycling, pp. 113–127, Springer, 1986.